Article

Investigation of the Cause-Effect Relationships between the Exothermic Reaction and the Microstructures of Reactive Ni-Al Particles Produced by High Energy Planetary Ball Milling

Christian Bernauer *, Sandra Grohmann, Philipp Angermann, Daniel Dickes [ID], Florian Holzberger, Pierre Amend and Michael F. Zaeh

Department of Mechanical Engineering, Institute for Machine Tools and Industrial Management (iwb), Technical University of Munich, 85748 Garching, Germany; sandra.grohmann@iwb.tum.de (S.G.); philipp.angermann@tum.de (P.A.); daniel.dickes@tum.de (D.D.); florian.holzberger@tum.de (F.H.); pierre.amend@tum.de (P.A.); michael.zaeh@iwb.tum.de (M.F.Z.)
* Correspondence: christian.bernauer@iwb.tum.de; Tel.: +49-(0)89-289-15568

Academic Editors: Dmitry Moskovskikh and Andreas Chrysanthou

Abstract: Reactive particles consisting of nickel and aluminum represent an adaptable heat source for joining applications, since each individual particle is capable of undergoing a self-sustaining exothermic reaction. Of particular interest are particles with intrinsic lamellar microstructures, as they provide large contact areas between the reactants nickel and aluminum. In this work, the exothermic reaction as well as the microstructure of such lamellar reactive particles produced by high energy planetary ball milling were investigated. Based on statistically designed experiments regarding the milling parameters, the heat of reaction was examined by means of differential scanning calorimetry (DSC). A statistical model was derived from the results to predict the heat of reaction as a function of the milling parameters used. This model can be applied to adjust the heat of reaction of the reactive particles depending on the thermal properties of the joining partners. The fabricated microstructures were evaluated by means of scanning electron microscopy (SEM). Through the development of a dedicated SEM image evaluation algorithm, a computational quantification of the contact area between nickel and aluminum was enabled for the first time. A weak correlation between the contact area and the heat of reaction could be demonstrated. It is assumed that the quantification of the contact areas can be further improved by a higher number of SEM images per sample. The findings obtained provide an essential contribution to enable reactive particles as a tailored heat source for joining applications.

Keywords: self-propagating high-temperature synthesis (SHS); high energy ball milling (HEBM); nickel aluminides; reactive particles; thermal analysis; microstructure

1. Introduction

Combustion synthesis, which is also known as self-propagating high-temperature synthesis (SHS), is a process in which at least two reactants, which are denoted as reactive system, are transformed into a product in a highly exothermic reaction [1,2]. SHS has been widely used for the synthesis of high-performance materials, typically employing homogeneous powder mixtures of the reactants [3,4]. However, the energy released by the exothermic reaction can also be used as an innovative and tailorable heat source, and thus SHS represents a promising approach for thermal joining applications.

One of the most widely studied reactive systems is the one consisting of nickel and aluminum. Nickel aluminides offer various advantageous characteristics, such as excellent mechanical properties and high-temperature resistance [1,5]. Multilayer systems, which consist of alternating layers of the reactants, are already commercially available for the Ni–Al system [6]. Moreover, reactive systems in the form of reactive particles were investigated [7]. In contrast to homogeneous powder mixtures, reactive particles provide the

advantage that each particle can react independently. A defined amount of energy can be released depending on various influencing factors, such as the stoichiometric ratio of the reactants contained. Important types of these reactive particles are core–shell structures obtained by wet chemical synthesis [8,9] as well as lamellar microstructures obtained by high energy ball milling (HEBM) of metallic powders [10,11]. When using a planetary ball mill, particles with an intrinsic structure similar to that of multilayer systems can be produced in an economical way [11–13]. Fine lamellar microstructures provide larger contact areas between the reactants than coarse ones. Planetary ball mills are commonly used for fine grinding and mechanical alloying of various materials, but it is also possible to specifically modify the microstructure of reactive particles [14].

With HEBM, the activation temperature of homogeneous Ni + Al powder mixtures can be significantly reduced, while the heat of reaction is increased [10,11]. This is not only caused by a reduction in particle size [10], but also by an increase of the contact area between nickel and aluminum due to the formation of lamellar microstructures within the particles [15–18]. The mechanisms involved in the formation of lamellar microstructures were discussed in detail in various studies. It was shown that flattening and cold welding of the metal particles occur during HEBM, causing the particle sizes to increase during milling [15,16,18,19]. Due to the higher ductility of aluminum, an aluminum matrix with embedded nickel regions is formed. During milling, the aluminum matrix hardens and thus mechanical impacts, e.g. of the milling balls, are transferred to the nickel regions. This leads to a gradual refinement [18,20]. The milling process can be affected by numerous parameters that determine the microstructure and the activation and reaction behavior of the obtained particles. Important parameters include the rotational speed, the resulting centrifugal acceleration, the milling time, the ball-to-powder (btp) ratio, and the size of the milling media [12,17,19]. However, differences in the equipment used often impede a direct comparison between the performed experimental studies.

For reactive particles produced by HEBM it was found that they can undergo an exothermic reaction without the formation of any liquid phases, whereas homogeneous powder mixtures form liquid intermediates under the same conditions [21]. In homogeneous Ni + Al powder mixtures, the exothermic reaction is initiated when the aluminum melts, which can be explained by a significant increase in the diffusion rate of solid nickel into liquid aluminum [18]. By increasing the contact area of the reactants through HEBM, the diffusion rate can become sufficiently high, even at lower temperatures, for a solid–solid reaction to occur. Therefore, the ignition temperature of homogeneous Ni + Al powder mixtures processed by HEBM can be significantly lower than the melting point of pure aluminum [17]. It is also important to note that HEBM can lead to contact areas between nickel and aluminum without any oxide layers [15–17]. For fine lamellar microstructures, which are associated with larger contact areas, the activation temperature declines [12,17,18,21].

Based on the findings of previous investigations, the following hypothesis is deduced: The activation and reaction behavior of the reactive particles might be predicted from the contact area between nickel and aluminum and could be adjusted through the milling parameters used. As a result, tailored reactive particles can be produced for thermal joining applications. Similar to Hadjiafxenti et al. [11], Gunduz et al. [22], and Lee et al. [23], the thermal material properties are determined using differential scanning calorimetry (DSC) in this work. In order to correlate the DSC measurements with the microstructures of reactive particles, an additional optical evaluation is required. The morphological properties can be investigated by scanning electron microscopy (SEM), which was done qualitatively in previous studies [10,18]. In this work, the presented SEM image evaluation algorithm is a key element, as it allows a computational determination of the contact area between the reactants.

2. Materials and Methods

2.1. Reactive Particle Manufacturing

The milling experiments were conducted with homogeneous powder mixtures of nickel (Thermo Fisher GmbH (Alfa Aesar), Kandel, Germany; 99.9% purity, 3–7 μm) and aluminum particles (New Materials Development GmbH, 99.7% purity, 4.8 μm) in an air atmosphere without any milling additives. To support this approach and to investigate the possible formation of oxide-rich phases, individual samples were investigated employing energy-dispersive X-ray spectroscopy (EDX). No increased oxygen concentration could be detected within the particles. Thus, the formation of oxide-rich phases could essentially be excluded. The molar ratio between nickel and aluminum was 1:1. The maximum speed of the planetary ball mill (Pulverisette 7 premium line, Fritsch GmbH, Idar-Oberstein, Germany) was set at 800 rpm, corresponding to a centrifugal acceleration of 70 g. The speed ratio of the sun wheel to the milling jars was 1:–2. A milling jar made of tempered steel with a volume of 20 mL and an inner radius of 23 mm was used together with milling balls that had diameters of 3 mm, 5 mm, and 10 mm and were made of the same material. The total mass of the milling balls for all sizes used was approximately 40 g. After each milling experiment, a cleaning procedure was carried out. This was necessary since adhesions of reactive particles on the milling balls and jar alter the milling parameters and cross-contaminate the samples produced. First, the milling balls and jar were treated chemically with a ten percent caustic soda solution (sodium hydroxide, 99% purity, Grüssing GmbH, Filsum, Germany), causing the aluminum to dissolve. Second, mechanical cleaning was carried out by placing the milling balls in the jar together with 4–8 g of SiO_2 and conducting a five minute milling cycle. If adhesions remained, the procedure was repeated.

In order to examine the influence of different milling parameters on the activation and reaction behavior of the reactive particles, four parameters and three factor levels each were studied: the rotational speed of the sun wheel n (650 min^{-1}, 725 min^{-1}, and 800 min^{-1}), the milling time t (15 min, 22.5 min, and 30 min), the ball diameter d (3 mm, 5 mm, and 10 mm), and the btp ratio r_{btp} (5, 7.5, and 10). Based on extensive preliminary tests, these four parameters were systematically varied following a central composite experimental design. In summary, 59 experiments were conducted with each yielding a distinct batch of reactive particles. The experimental plan can be found in Appendix A (Table A1).

2.2. Differential Scanning Calorimetry

The thermal properties of the reactive particles were determined using DSC. For this purpose, the measuring device TGA/DSC3+ (SDTA sensor, Mettler-Toledo GmbH, Gießen, Germany) was used with 150 μL crucibles made of Al_2O_3. The software STARe V14.00 was utilized for the evaluation of the measurements. All DSC experiments were performed in an argon atmosphere, as the use of air and nitrogen led to significant oxidation and nitration, respectively, and thus an increase in the sample mass. In order to remove any air present in the sample chamber, isothermal rinsing was performed at 298.15 K for 15 min at an argon flow rate of 50 mL/min before all measurements. This was followed by continuous heating, during which the temperature was increased from 298.15 K to 1273.15 K at a heating rate of 30 K/min and an argon flow rate of 20 mL/min.

Sample masses of 100 mg were weighed in with a maximum deviation of ±0.5 mg. The measurements were repeated twice for each sample. After the measurement was completed, the crucible was cleaned with a glass fiber eraser and a propane torch. The method used to determine the heat of reaction Q_r from the DSC measurements is illustrated in Figure 1, where Φ_r is the reaction heat flow and Φ_{bl} is the baseline heat flow.
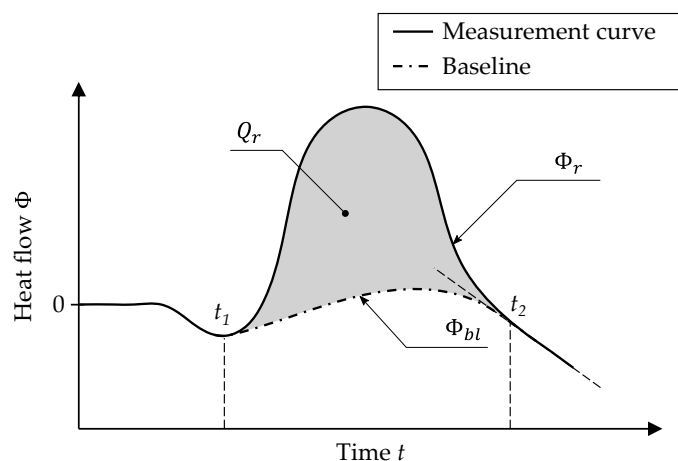
Figure 1. Procedure for determining the heat of reaction using the measurement curve and a constructed baseline.

The heat released from the sample corresponds to the integral of the heat flow over time subtracted by the integral of the baseline, which represents a measurement curve without consideration of thermal transformation processes or reactions of the material examined [24]. Since the baseline is dependent on changes in the specific heat capacity of the reactive particles during the measurement, it cannot be determined by repeating the experiment with the same sample and must therefore be constructed. In order to obtain comparable results, a systematic procedure was developed. The onset point t_1 was set to the local minimum at the beginning of the measurement. At the point where the change of heat flow was constant for the first time after the reaction, the endset point t_2 was set. Between t_1 and t_2 the baseline was interpolated as a spline. Thus, the heat of reaction was determined as [24]

$$Q_r = \int_{t_1}^{t_2} \Phi_r - \Phi_{bl} \; dt \tag{1}$$

It is important to note that both the manual setting of the integration limits and the interpolation of the baseline as a spline have an effect on the determined values. Therefore, the procedure was carried out uniformly for all experiments in order to guarantee the comparability of the results.

2.3. SEM Image Evaluation Algorithm

For the analysis of the microstructure of the reactive particles on the basis of SEM images, a dedicated SEM image evaluation algorithm was developed. This was necessary since no commercially available software could fully meet the specific requirements for image processing and maximum flexibility for adapting the algorithm was desired. As this algorithm enables an automated quantification of the contact areas between nickel and aluminum, it represents a significant added value compared to the state of the art. Micrographs of the fabricated reactive particles were generated using a scanning electron microscope (TM3030 plus, Hitachi High-Tech Corporation, Tokyo, Japan) with an electrode voltage of 15 kV in standard observation mode.

Uniform SEM images had to be obtained for all reactive particles produced in order to systematically evaluate the microstructures. Therefore, a 1500-fold magnification was chosen, and the guidelines listed below were followed:

- The recorded SEM images had to be sharp.
- No epoxy resin could be visible.
- No outer edges of the reactive particles could be visible.
- The selection of the embedded reactive particles to be imaged was randomized.

A computer-aided evaluation was required for an objective and efficient analysis of the generated SEM images. Consequently, an image processing algorithm was developed

to quantify the lamellar microstructure within the reactive particles. The approach is based on the hypothesis that the contact area between nickel and aluminum correlates with the length of the boundary line visible in the two-dimensional SEM images. Thus, the overall length of the boundary lines for reactive particles with finer lamellar microstructures should be higher. As a suitable parameter for quantifying this length, the number of pixels (NOP) comprising the boundary line between nickel and aluminum was chosen. The basic structure of the SEM image evaluation algorithm is shown schematically in Figure 2.
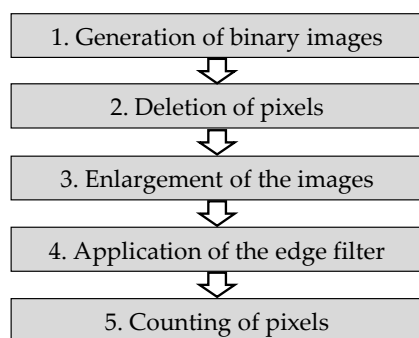

Figure 2. Steps of the developed SEM image evaluation algorithm.

The SEM image evaluation algorithm was developed and executed in MATLAB 2017b (MathWorks, Natick, MA, USA). First, a binary image was generated from the original grayscale SEM image, where areas consisting of aluminum are colored black and areas consisting of nickel are colored white. This was achieved by computing a threshold using Otsu's method [25], based on which the binary image is generated. For this, the algorithm first computes the intensity histogram of the corresponding grayscale image and subsequently determines the threshold such that the intraclass variance of the two resulting pixel classes is minimized. The functions *greythresh* and *imbinarize* were used. Subsequently, areas with up to three white pixels, which are caused by image noise and would distort the measurement result, were deleted. Furthermore, a Sobel operator was used to display only the edges of the white areas within the binary image. To increase accuracy, the binary image was enlarged from 1280×980 pixels to 5120×3840 pixels, since only edges of white areas with at least 3×3 pixels could be displayed. In Figure 3, the procedure is visualized exemplarily using a section of an SEM image.
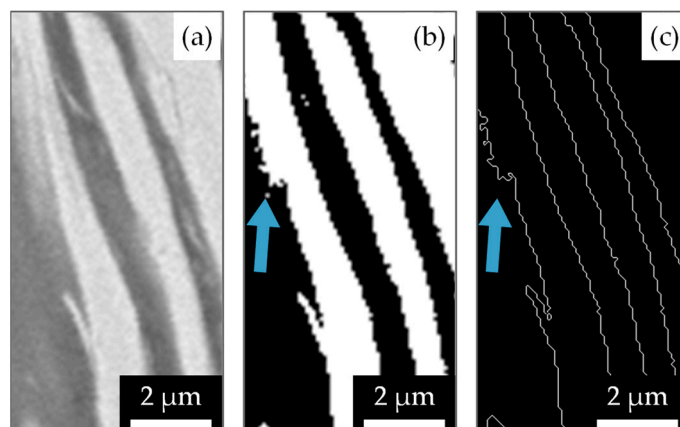
Figure 3. Generation of the boundary lines based on the initial greyscale SEM image: (**a**) section of the original SEM image; (**b**) generation of a binary image (step 1); (**c**) deletion of pixels, enlargement of the image, and application of the edge filter (steps 2–4).

The boundary lines generated by the algorithm and the ones of the original SEM image were in very good agreement. Lastly, the remaining white pixels of the boundary

lines are counted and stored in an array. For the reactive particles obtained from the milling experiments, three SEM images were taken and processed. Due to the total high number of SEM images, the algorithm was developed to enable a fully automatic determination of the NOP for all selected files.

3. Results and Discussion

3.1. Thermal Characterization by Means of DSC

The use of reactive particles as an innovative heat source in joining applications requires knowledge about their thermal properties. In the following, the findings of the DSC analyses are thus presented. In Figure 4, the measurement curve of an exemplary DSC scan is shown.
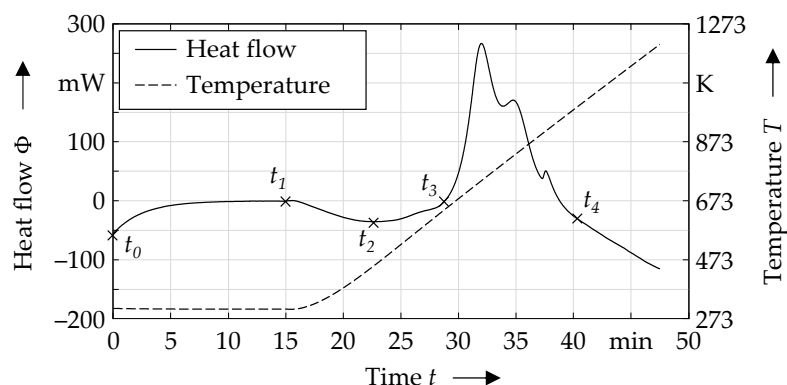

Figure 4. Heat flow and temperature curve for a DSC measurement (experiment no. 41, see Appendix A).

During isothermal rinsing with argon ($t_0 = 0$ min to $t_1 = 15$ min), an endothermic heat flow occurred, which can be explained by the heating of the material sample from room temperature to the specified temperature of 298.15 K. After 15 min, the heating began, in which heat was initially still being absorbed by the sample. The heat flow reached a local minimum after $t_2 = 23$ min and was zero for the first time after $t_3 = 29$ min, indicating an exothermic reaction after this point. The reaction was completed after $t_4 = 40.5$ min, which was shown by the constant decline of the heat flow. Among the samples analyzed, different shapes of the measurement curves with characteristic peaks were observed within the interval $t_2 < t < t_4$. These shapes are considered as a consequence of the microstructure of the reactive particles resulting from the different milling parameters used. In Figure 5 three typical forms are depicted by which a classification was made.
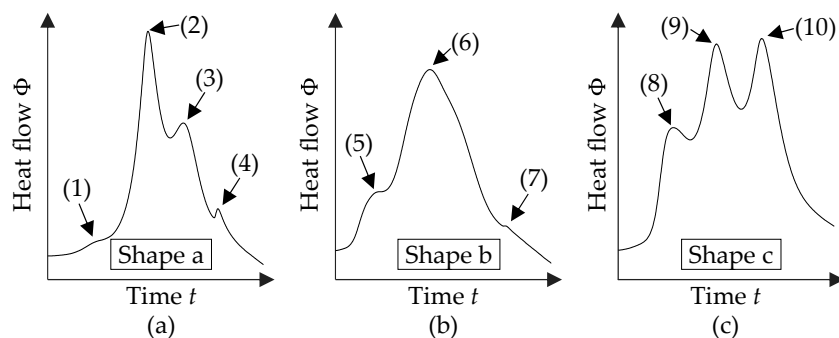

Figure 5. Typical measurement curves for $t_2 < t < t_4$: (**a**) experiment no. 58; (**b**) experiment no. 30; (**c**) experiment no. 47.

The shape in Figure 5a consists of four peaks, where peak (2) and (3) are most pronounced and peak (3) is smaller than peak (2). Figure 5b shows another common form, in

which a small initial peak (5) is followed by a highly dominant one (6) and an even smaller peak (7) at the end. The characteristic shape in Figure 5c is defined by three peaks with the first one (8) having a smaller maximum than the two following peaks, (9) and (10), which are approximately equal in size. The individual peaks indicate phase transformations of the Ni–Al system. However, for an exact evaluation of the phase transformation processes, analyses of quenched samples in combination with XRD evaluations would be necessary. Measurement curves similar to the ones shown above were also observed by Manukyan et al. [18]. Some samples exhibited mixed forms, which represent superpositions between the three forms and are referred to as a-b and b-c. Such superpositions have also been described by Thiers et al. [26] for certain heating rates due to various effects such as phase transformations. The occurrence of different measurement curves was also observed for multilayer systems, where the layer thickness of the reactants is the most important influencing factor [27,28]. For particles produced by planetary ball milling, it was shown by Manukyan et al. [18] that different DSC measurement curves occur, depending on whether a coarse or a fine lamellar microstructure is present. This relationship is examined in more detail in Section 3.2. The assigned shapes for all samples as well as the calculated heat of reactions are given in Table 1.

Table 1. Heat of reactions of the samples and assigned shapes of the measurement curve.

Exp. No.	Q_r in J/g	Shape	Exp. No.	Q_r in J/g	Shape	Exp. No.	Q_r in J/g	Shape
1	914	b	21	920	b	41	740	a
2	801	a	22	918	a-b	42	872	a-b
3	858	a-b	23	829	b-c	43	865	a-b
4	864	a-b	24	800	b	44	823	c
5	890	b	25	880	a	45	837	a
6	771	b	26	872	b	46	840	a
7	743	b	27	831	b	47	854	c
8	733	b	28	894	b	48	796	a
9	796	b	29	850	b	49	839	a
10	752	a	30	851	b	50	925	c
11	875	a	31	876	a-b	51	872	a
12	827	a-b	32	871	b	52	874	a
13	1004	b-c	33	906	a-b	53	769	a
14	785	a	34	938	c	54	851	a
15	803	c	35	969	c	55	845	a
16	768	a-b	36	858	a	56	844	a
17	843	c	37	834	a-b	57	803	a
18	884	a-b	38	935	b-c	58	800	a
19	965	b	39	918	c	59	937	c
20	800	b	40	886	b-c			

As can be seen in Table 1, the determined heat of reactions ranged between 733 J/g and 1004 J/g, which is considerably lower than the theoretical heat of formation for NiAl of 1382 J/g [1]. This may be related to the fact that in practice an ideal lamellar microstructure (e.g., equal lamellar thicknesses) is difficult to achieve, resulting in incomplete reactions due to long diffusion distances. Furthermore, milling in an air atmosphere may result in the presence of impurities due to the formation of aluminum and nickel oxides. Accordingly, the heat of reaction could be further increased by conducting the milling process in an argon atmosphere. In milling experiments by Lee et al. [23], which were likewise conducted in an air atmosphere, values for the heat of reaction between 906 J/g and 1150 J/g were obtained on the basis of DSC analyses. However, this comparison must be considered critically due to the different milling equipment used as well as the distinct method of analysis. The procedure of the DSC analysis also influences the determined heat of reaction. It should be noted here that the standardized procedure allows good comparability of the results within the present work. Nevertheless, it is worth mentioning that the use of

bomb calorimetry would allow an even more accurate measurement of the heat of reaction than DSC.

In order to correlate the shape of the measurement curve with the determined heat of reaction, the mean values $\overline{Q}$ for the samples of the corresponding category (shape) are given in Table 2. The highest average heats of reaction were found for shape c as well as for the mixed forms b-c.

Table 2. Mean heat of reaction depending on the shape of the measurement curve.

Shape acc. to Figure 5	Quantity	$\overline{Q}$ in J/g	Standard Deviation
all	59	852	60
a	19	824	42
b	15	842	66
c	9	890	56
a-b	11	861	39
b-c	4	913	65

Based on these results, a correlation between the heat of reaction and the shape of the curve was concluded. The highest mean heats of reaction were measured for the shapes c and b-c. With few exceptions, all peaks occurred at temperatures below the melting point of aluminum. Therefore, the reactions can be classified as solid–solid reactions. Peak (4) and peak (7), respectively, in Figure 5 were observed at approximately 933 K and thus can be attributed to solid–liquid reactions with the melting of aluminum.

Furthermore, it was investigated how the different milling parameters affect the heat of reaction of the reactive particles. In order to describe the correlation between the influencing factors and the heat of reaction for the investigated four-dimensional parameter space, a model equation was determined by means of a multiple regression analysis using MATLAB R2017b. In order to quantify the influence of each milling parameter and to identify existing factor correlations, an analysis of variance (ANOVA) was carried out. Table 3 shows the results.

Table 3. Results of the ANOVA for the correlation between the heat of reaction and the milling parameters.

Source	Sum of Squares	Degrees of Freedom	Mean Square	F-Value	p-Value
n	40,682	2	20,341	11.55	0.0001
t	38,110	2	19,055	10.82	0.0001
r_{btp}	4980	2	2490	1.41	0.2529
d	26,049	2	13,025	7.39	0.0015
Error	88,076	50	1762		
Total	203,812	58			

For the data investigated, the rotational speed, the milling time, and the ball diameter each have a p-value of less than 0.05 and can thus be considered as significant influencing factors on the heat of reaction. No significant interactions between the individual parameters could be determined. A quadratic model without interactions was applied for the regression analysis, whereby non-significant terms with p-values below 0.05 were systematically removed. The final model is given by

$$Q_r = 262.58 + 0.415\,n + 3.989\,t + 71.067\,d - 5.197\,d^2, \tag{2}$$

where the coefficient of determination R^2 was 0.514. The ball diameter is the only parameter that shows a negative quadratic influence, which indicates that the use of small and large milling balls tends to result in a lower heat of reaction than the use of milling balls with a medium diameter of 5 mm. This may be related to the movement pattern of the milling balls within the milling jar. It can be assumed that for specific milling ball diameters an increased circular movement of the milling balls compared to the free-flying movement

occurs, as described by Rogachev et al. [14] and Baláž [29]. With the circular movement, the milling balls merely roll along the inner edge of the jar, so that energy is not transferred into the material through impact loading, but rather through shearing. As a result, the energy input into the reactive particles is reduced despite the overall mass of the milling balls being identical for all diameters. It should be noted that smaller milling balls also tended to produce smaller reactive particles. It can be assumed that these smaller reactive particles lead to a lower ignition temperature and a higher maximum reaction temperature. However, the effect of particle sizes has not been considered in detail in the investigations carried out.

Generally, it can be expected that a sufficiently high energy input into the powder materials during milling will result in gradual alloying and the formation of NiAl, which reduces the heat of reaction determined through DSC analysis. This might also be an explanation for the reduction of the heat of reaction with large milling ball diameters. However, a partial reaction of the lamellar particles could only be found for experiment no. 17 (see Figure 6), where all parameters were at the highest factor level ($n = 800$ min^{-1}, $t = 30$ min, $d = 10$ mm, $r_{btp} = 10$). The assumption that the particles reacted partially in this experiment is based on the fact that for unreacted particles, the areas of Ni and Al can usually be distinguished from each other very well based on their intensity in the grayscale image. In contrast, a uniform grey value is present in reacted particles due to the uniform distribution of nickel and aluminum resulting from the formation of intermetallic phases. The sporadic occurrence of reacted particles at a high energy input shows that the chosen parameter window was sufficiently large to maximize the reactivity of the reactive particles, as a further increase is likely to result in an alloying in the milling jar.
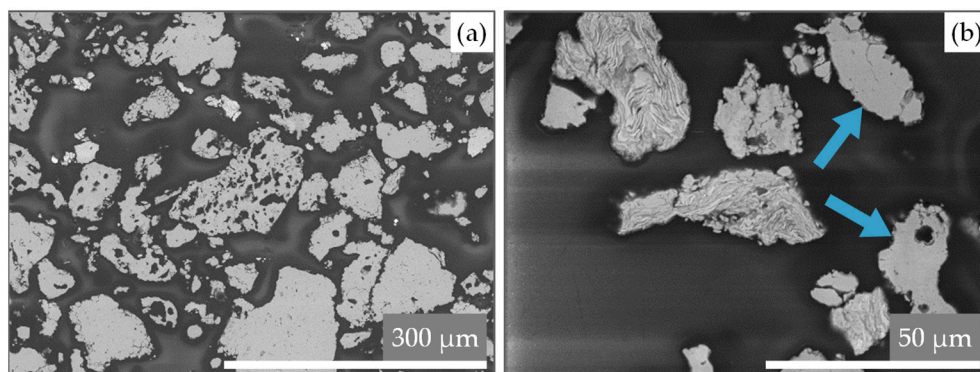

Figure 6. SEM images of reacted particles in exemplary areas of the sample (experiment no. 17). (**a**) 300-fold magnification; (**b**) 1500-fold magnification

3.2. Correlation between the Microstructure and the Heat of Reaction

The correlation between the microstructure of the reactive particles and the heat of reaction was investigated on the basis of the SEM image evaluation algorithm. As discussed in Section 1, it can be derived from different studies that more refined lamellae lead to an improved activation and reaction behavior due to the higher contact area between nickel and aluminum [17,18]. In contrast, coarse structures with larger nickel or aluminum regions might not react completely due to the longer diffusion distances [30]. This leads to the hypothesis that the heat of reaction can be predicted on the basis of the existing contact area and vice versa. It should be taken into account that higher factor levels of the milling parameters result in a higher energy input into the reactive particles, which promotes the formation of lamellar microstructures. If this energy input is too high, partial reactions in the milling jar may occur, causing the measured heat of reaction to decline. However, since only in experiment no. 17 a few reacted particles could be observed, it can be assumed that the energy input within the selected parameter window was generally not sufficient for mechanical alloying to occur.

In order to quantify the microstructures of the manufactured reactive particles, SEM images according to the procedure described in Section 2.3 were taken for all samples of reactive particles, and the developed SEM image evaluation algorithm was deployed. This allowed for the determination of the NOP, which was used as a measure for the contact area between nickel and aluminum. The average NOP of the three images taken for each sample are given in Table 4.

Table 4. Number of pixels (NOP) for the conducted experiments.

Exp. No.	NOP (Mean) $\times 10^5$	Exp. No.	NOP (Mean) $\times 10^5$	Exp. No.	NOP (Mean) $\times 10^5$
1	3.98	21	5.49	41	2.40
2	2.35	22	3.25	42	3.10
3	3.31	23	5.98	43	3.88
4	3.24	24	3.54	44	9.13
5	4.12	25	4.60	45	3.03
6	4.54	26	4.34	46	4.61
7	4.82	27	3.88	47	8.78
8	4.65	28	8.37	48	3.26
9	6.13	29	4.54	49	3.76
10	1.99	30	3.85	50	9.59
11	2.79	31	8.90	51	4.46
12	3.27	32	3.89	52	4.83
13	4.33	33	5.17	53	2.61
14	3.50	34	10.20	54	3.93
15	6.61	35	9.63	55	6.37
16	5.74	36	5.59	56	4.27
17	8.76	37	3.48	57	2.50
18	3.23	38	3.29	58	2.39
19	5.33	39	5.09	59	7.44
20	3.47	40	7.53		

In addition, for the samples with the highest and the lowest mean NOP, an SEM image is shown in Figure 7.
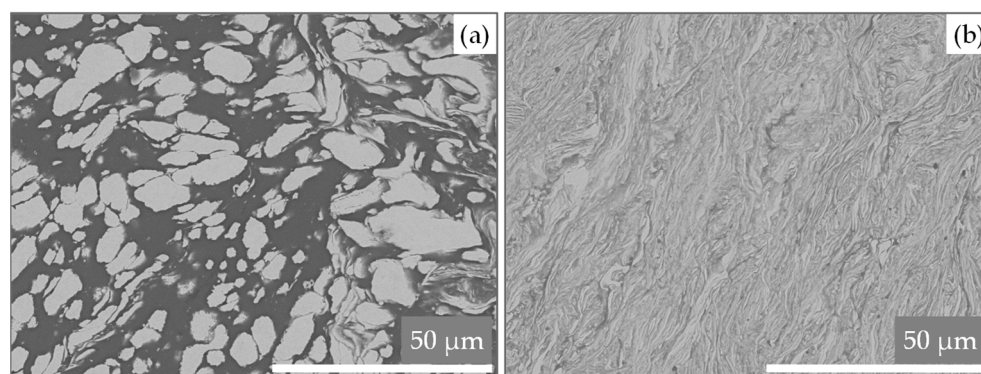

Figure 7. SEM images used for the evaluation of the sample with the lowest ((**a**), experiment no. 10) and the highest ((**b**), experiment no. 34) mean NOP.

It should be noted that the obtained NOP does not necessarily represent an exact measure for the total contact areas within individual particles. This is due to the fact that the images show a random two-dimensional cross-section of the reactive particles as a result of the sample preparation procedure. This was partly compensated by the described averaging of the three images for each experiment. Therefore, the NOP must be considered as a valuable tool to quantify and thus compare the characteristics of the lamellar microstructures within the reactive particles.

Finally, the NOP values were correlated with the heat of reaction. A linear regression yielded a coefficient of determination of 0.127. This indicates that a weak correlation existed, but it was not particularly pronounced. Figure 8 shows the regression model and the observations. A slight trend can be seen, although there were many significant outliers.
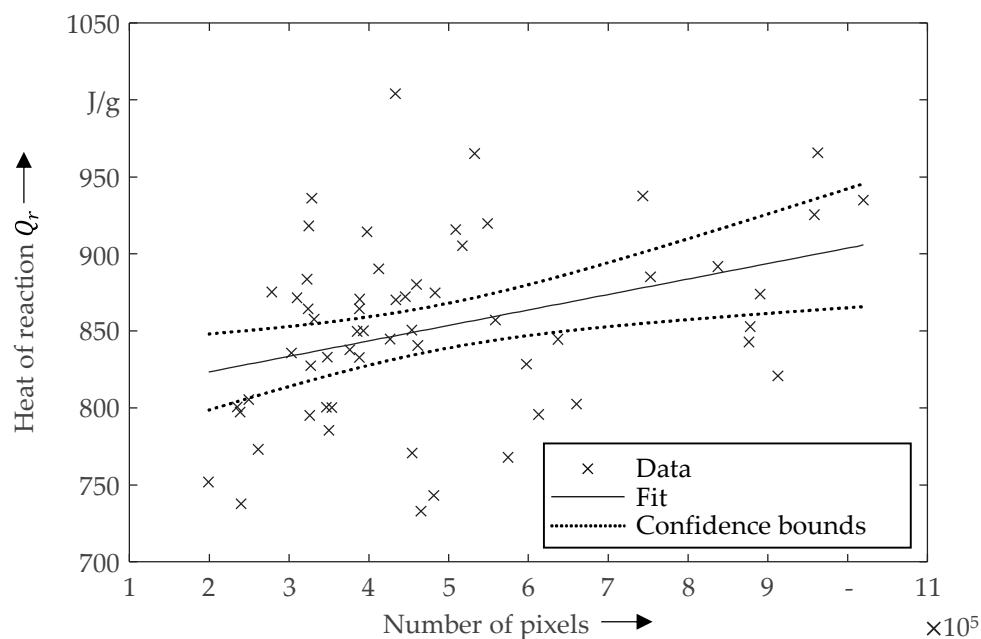

Figure 8. Linear regression model for the heat of reaction as a function of the NOP.

An explanation for the high dispersion of the values is that despite multiple measurements per sample and averaging, it cannot be guaranteed that the NOP is always represented accurately. Both the sample preparation as well as the varying degree of formation of the lamellar microstructures within individual reactive particles have a significant influence. Thus, the hypothesis that the heat of reaction may be predicted based on the determined contact area cannot be confirmed conclusively on the basis of the method used. Nevertheless, it can be derived that the heat of reaction generally increases with more refined lamellar microstructures. For further improvement of the estimation of the contact area, a larger number of images should be used in future work.

It is also noticeable that the determined NOP values showed a significantly higher overall variance than the values for the heat of reaction. While the minimum determined NOP was only 20% of the maximum NOP, the lowest heat of reaction corresponded to 73% of the largest one. An explanation for this is provided in the following: The Ni–Al system can undergo an exothermic reaction under a wide variety of conditions. With a coarse structure, there is already sufficient contact between nickel and aluminum, and even in homogeneous Ni + Al powder mixtures, a reaction can be initiated. Yet, the reactivity of the reactive particles is further enhanced by the refinement of the lamellar microstructure, but not to the same extent as the contact area increases.

4. Conclusions

In this study, different reactive particles consisting of nickel and aluminum were produced by high energy ball milling and were investigated regarding their reactivity as well as their intrinsic microstructure. In statistically designed experiments, the milling parameters rotational speed, milling time, ball diameter, and ball-to-powder ratio were varied and the particles produced were examined by means of DSC analyses concerning the released heat of reaction. A model equation was determined in order to describe the correlation between the milling parameters and the heat of reaction. Further, an SEM image evaluation algorithm was developed. This algorithm represents a significant added value,

as it allows a quantification of the contact areas between nickel and aluminum within individual reactive particles using the number of boundary line pixels as an auxiliary value. The proposed hypothesis, that the heat of reaction can be predicted from the contact area, could not be fully confirmed with the evaluation method used. A weak correlation between the heat of reaction and the degree of refinement of the lamellar microstructures was found, which promotes further investigations. Therefore, in future work, additional dynamic simulations of the formation of the contact areas during milling will be carried out and the variation of further parameters such as the molar ratio between nickel and aluminum will be investigated. Furthermore, XRD analyses should be conducted to allow a detailed investigation of the intermetallic phases after the reactions to complement the results of this work. Another important aspect of research, that should be considered in future studies, is the effect of particle sizes on the activation and reaction behavior. In this context, the use of compacted particles should also be investigated, as this can further improve the reaction characteristics. The findings of this work can be used to further enable reactive particles as a tailored heat source for thermal joining applications, where they can be an advantageous alternative compared to the already established multilayer systems in terms of cost, flexibility, and scalability. Due to their thermal properties, reactive particles provide significant benefits for joining technologies such as welding, soldering, or adhesive bonding.

Author Contributions: Conceptualization, S.G. and C.B.; methodology, S.G. and C.B.; software, S.G., P.A. (Philipp Angermann), and D.D.; validation, S.G. and C.B.; formal analysis, C.B. and S.G.; investigation, S.G., P.A. (Philipp Angermann), D.D., F.H., and P.A. (Pierre Amend); resources, M.F.Z.; data curation, S.G., C.B., P.A. (Philipp Angermann), D.D., F.H., and P.A. (Pierre Amend); writing—original draft preparation, C.B.; writing—review and editing, S.G. and M.F.Z.; visualization, C.B.; supervision, M.F.Z.; project administration, S.G. and M.F.Z.; funding acquisition, S.G. and M.F.Z. All authors have read and agreed to the published version of the manuscript.

Conflicts of Interest: The authors declare no conflict of interest. The funders had no role in the design of the study; in the collection, analyses, or interpretation of data; in the writing of the manuscript; or in the decision to publish the results.

Appendix A

Table A1. Experimental plan for the high energy ball milling of Ni–Al powders in a 1:1 molar ratio with a systematic variation of milling parameters.

Exp. No.	n in rpm	t in min	r_{btp}	d in mm	Exp. No.	n in rpm	t in min	r_{btp}	d in mm
1	725	22.5	7.5	5	31	800	30	7.5	3
2	650	15	5	3	32	650	30	7.5	3
3	800	15	5	3	33	725	30	5	5
4	650	30	5	3	34	725	30	10	5
5	800	30	5	3	35	800	30	7.5	5
6	650	15	10	3	36	650	30	7.5	5
7	800	15	10	3	37	800	15	5	5
8	650	30	10	3	38	800	30	5	5
9	800	30	10	3	39	800	15	10	5
10	650	15	5	10	40	800	30	10	5
11	800	15	5	10	41	650	15	5	5
12	650	30	5	10	42	650	30	5	5
13	800	30	5	10	43	650	15	10	5
14	650	15	10	10	44	800	15	10	10
15	800	15	10	10	45	650	22.5	7.5	10
16	650	30	10	10	46	725	30	5	10
17	800	30	10	10	47	725	30	10	10
18	650	22.5	7.5	5	48	725	15	7.5	10
19	800	22.5	7.5	5	49	725	22.5	5	10
20	725	15	7.5	5	50	800	30	7.5	10
21	725	30	7.5	5	51	650	30	7.5	10
22	725	22.5	5	5	52	800	15	7.5	10
23	725	22.5	10	5	53	650	15	7.5	10
24	725	22.5	7.5	3	54	725	15	10	10
25	725	22.5	7.5	10	55	650	22.5	10	10
26	800	22.5	7.5	3	56	800	22.5	5	10
27	725	30	5	3	57	650	22.5	5	10
28	725	30	10	3	58	725	15	5	10
29	725	30	7.5	3	59	800	22.5	10	10
30	725	22.5	10	3					

References

1. Morsi, K. Review: Reaction synthesis processing of Ni–Al intermetallic materials. *Mater. Sci. Eng. A* **2001**, *299*, 1–15. [CrossRef]
2. Merzhanov, A.G. The chemistry of self-propagating high-temperature synthesis. *J. Mater. Chem.* **2004**, *14*, 1779–1786. [CrossRef]
3. Merzhanov, A.G. History and recent developments in SHS. *Ceram. Int.* **1995**, *21*, 371–379. [CrossRef]
4. Rogachev, A.S.; Mukasyan, A.S. *Combustion for Material Synthesis*; CISP; CRC Press: Boca Raton, FL, USA, 2015; ISBN 978-1-4822-3952-2.
5. Deevi, S.C.; Sikka, V.K. Nickel and iron aluminides: An overview on properties, processing, and applications. *Intermetallics* **1996**, *4*, 357–375. [CrossRef]
6. Theodossiadis, G.D.; Zaeh, M.F. Assessment of the technological potential and maturity of a novel joining technique based on reactive nanofoils. *Prod. Eng. Res. Dev.* **2017**, *11*, 237–243. [CrossRef]
7. Grohmann, S.; Langhans, G.; Reindl, A.; Sidarava, V.; Zaeh, M.F. Investigation of reactive bimetallic Ni–Al particles as a heat source for microwave-assisted joining. *J. Mater. Process. Technol.* **2020**, *282*, 116637. [CrossRef]
8. Schreiber, S.; Theodossiadis, G.D.; Zaeh, M.F. Combustion synthesis of reactive nickel-aluminum particles as an innovative approach for thermal joining applications. *IOP Conf. Ser. Mater. Sci. Eng.* **2017**, *181*, 1–8. [CrossRef]
9. Schreiber, S.; Zaeh, M.F. Electroplating of aluminium microparticles with nickel to synthesise reactive core-shell structures for thermal joining applications. *IOP Conf. Ser. Mater. Sci. Eng.* **2018**, *373*, 1–9. [CrossRef]
10. Rogachev, A.S.; Shkodich, N.F.; Vadchenko, S.G.; Baras, F.; Kovalev, D.Y.; Rouvimov, S.; Nepapushev, A.A.; Mukasyan, A.S. Influence of the high energy ball milling on structure and reactivity of the Ni+Al powder mixture. *J. Alloy. Compd.* **2013**, *577*, 600–605. [CrossRef]
11. Hadjiafxenti, A.; Gunduz, I.E.; Kyratsi, T.; Doumanidis, C.C.; Rebholz, C. Exothermic reaction characteristics of continuously ball-milled Al/Ni powder compacts. *Vacuum* **2013**, *96*, 73–78. [CrossRef]
12. Hadjiafxenti, A.; Gunduz, I.E.; Tsotsos, C.; Kyratsi, T.; Doumanidis, C.C.; Rebholz, C. Synthesis of reactive Al/Ni structures by ball milling. *Intermetallics* **2010**, *18*, 2219–2223. [CrossRef]
13. Cherukara, M.J.; Germann, T.C.; Kober, E.M.; Strachan, A. Shock loading of granular Ni/Al composites. Part 2: Shock-induced chemistry. *J. Phys. Chem. C* **2016**, *120*, 6804–6813. [CrossRef]
14. Rogachev, A.S.; Moskovskikh, D.O.; Nepapushev, A.A.; Sviridova, T.A.; Vadchenko, S.G.; Rogachev, S.A.; Mukasyan, A.S. Experimental investigation of milling regimes in planetary ball mill and their influence on structure and reactivity of gasless powder exothermic mixtures. *Powder Technol.* **2015**, *274*, 44–52. [CrossRef]
15. White, J.D.E.; Reeves, R.V.; Son, S.F.; Mukasyan, A.S. Thermal explosion in Al-Ni system: Influence of mechanical activation. *J. Phys. Chem. A* **2009**, *113*, 13541–13547. [CrossRef]
16. Mukasyan, A.S.; White, J.D.E.; Kovalev, D.Y.; Kochetov, N.A.; Ponomarev, V.I.; Son, S.F. Dynamics of phase transformation during thermal explosion in the Al–Ni system: Influence of mechanical activation. *Phys. B Condens. Matter* **2010**, *405*, 778–784. [CrossRef]
17. Shuck, C.E.; Mukasyan, A.S. Reactive Ni/Al nanocomposites: Structural characteristics and activation energy. *J. Phys. Chem. A* **2017**, *121*, 1175–1181. [CrossRef]
18. Manukyan, K.V.; Mason, B.A.; Groven, L.J.; Lin, Y.-C.; Cherukara, M.; Son, S.F.; Strachan, A.; Mukasyan, A.S. Tailored reactivity of Ni+Al nanocomposites: Microstructural correlations. *J. Phys. Chem. C* **2012**, *116*, 21027–21038. [CrossRef]
19. Suryanarayana, C.; Al-Aqeeli, N. Mechanically alloyed nanocomposites. *Prog. Mater. Sci.* **2013**, *58*, 383–502. [CrossRef]
20. Gu, Z.; Cui, Q.; Chen, J.; Buckley, J.; Ando, T.; Erdeniz, D.; Wong, P.; Hadjiafxenti, A.; Epaminonda, P.; Gunduz, I.E.; et al. Fabrication, characterization and applications of novel nanoheater structures. *Surf. Coat. Technol.* **2013**, *215*, 493–502. [CrossRef]
21. Kovalev, D.Y.; Kochetov, N.A.; Ponomarev, V.I.; Mukasyan, A.S. Effect of mechanical activation on thermal explosion in Ni-Al mixtures. *Int. J. Self-Propag. High-Temp. Synth.* **2010**, *19*, 120–125. [CrossRef]
22. Gunduz, I.E.; Kyriakou, A.; Vlachos, N.; Kyratsi, T.; Doumanidis, C.C.; Son, S.; Rebholz, C. Spark ignitable Ni–Al ball-milled powders for bonding applications. *Surf. Coat. Technol.* **2014**, *260*, 396–400. [CrossRef]
23. Lee, H.-Y.; Kim, T.-J.; Cho, Y.-J. Application of ball-milled powder mixture to intermetallics coating through reaction synthesis. *Met. Mater. Int.* **2013**, *19*, 1289–1293. [CrossRef]
24. Höhne, G.W.H.; Hemminger, W.; Flammersheim, H.-J. *Differential Scanning Calorimetry*, 2nd ed.; Springer: Berlin, Germany, 2003; ISBN 354000467x.
25. Otsu, N. A threshold selection method from gray-Level histograms. *IEEE Trans. Syst. Man Cybern.* **1979**, *9*, 62–66. [CrossRef]
26. Thiers, L.; Mukasyan, A.S.; Varma, A. Thermal explosion in Ni-Al system: Influence of reaction medium microstructure. *Combust. Flame* **2002**, *131*, 198–209. [CrossRef]
27. Knepper, R.; Snyder, M.R.; Fritz, G.; Fisher, K.; Knio, O.M.; Weihs, T.P. Effect of varying bilayer spacing distribution on reaction heat and velocity in reactive Al/Ni multilayers. *J. Appl. Phys.* **2009**, *105*, 083504-1–083504-9. [CrossRef]
28. Simões, S.; Viana, F.; Ramos, A.S.; Vieira, M.T.; Vieira, M.F. Anisothermal solid-state reactions of Ni/Al nanometric multilayers. *Intermetallics* **2011**, *19*, 350–356. [CrossRef]
29. Baláž, P. *Mechanochemistry in Nanoscience and Minerals Engineering*; Springer: Berlin, Germany, 2008; ISBN 978-3-540-74855-7.
30. Stover, A.K.; Krywopusk, N.M.; Fritz, G.M.; Barron, S.C.; Gibbins, J.D.; Weihs, T.P. An analysis of the microstructure and properties of cold-rolled Ni:Al laminate foils. *J. Mater. Sci.* **2013**, *48*, 5917–5929. [CrossRef]